3DGPS: A 3D Differentiable-Gaussian-based Planning Strategy for Liver Tumor Cryoablation

Ce Wang[13*], Xiaoyu Huang[2*], Yaqing Kong[24*], Qian Li[1*], You Hao[1(✉)], and Xiang Zhou[2(✉)]

[1] Key Laboratory of Intelligent Information Processing, Institute of Computing Technology, Chinese Academy of Sciences (CAS), Beijing 100190, China
[2] Department of Interventional Therapy, National Cancer Center/National Clinical Research Center for Cancer/Cancer Hospital, Chinese Academy of Medical Sciences and Peking Union Medical College, Beijing 100021, China.
[3] Suzhou Institute of Intelligent Computing Technology, CAS, Suzhou, China
[4] Department of Interventional Radiology, Fujian Medical University Union Hospital, Fuzhou, China
haoyou@ict.ac.cn, zhou.xiang@yeah.net

Abstract. Effective preoperative planning is crucial for successful cryoablation of liver tumors. However, conventional planning methods rely heavily on clinicians' experience, which may not always lead to an optimal solution due to the intricate 3D anatomical structures and clinical constraints. Lots of planning methods have been proposed, but lack interactivity between multiple probes and are difficult to adapt to diverse clinical scenarios. To bridge the gap, we present a novel **3**D **D**ifferentiable-**G**aussian-based **P**lanning **S**trategy (3DGPS) for cryoablation of liver tumor considering both the probe interactivity and several clinical constraints. Especially, the problem is formulated to search the minimal circumscribed tumor ablation region, which is generated by multiple 3D ellipsoids, each from one cryoprobe. These ellipsoids are parameterized by the differentiable Gaussians and optimized mainly within two stages, fitting and circumscribing, with formulated clinical constraints in an end-to-end manner. Quantitative and qualitative experiments on LiTS and in-house datasets verify the effectiveness of 3DGPS.

Keywords: 3D ellipsoids · Differentiable Gaussians · Deep learning · Tumor cryoablation planning · Liver tumor.

1 Introduction and motivation

Cryoablation is a minimally invasive therapy technique that inactivates tumors at extremely low temperature via cryoprobes, as green arrows in Fig. 1, which offers several advantages, such as the inherent analgesic qualities of hypothermia, the capacity to ablate a large zone in a single session, and real-time visibility via intraoperative CT [6, 16, 18]. During cryoablation, the clinician punctures probes

[*] These authors contributed equally to this work.

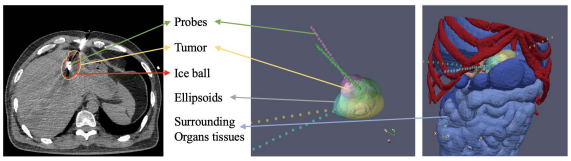

Fig. 1: The real-world example and the visual planning result of 3DGPS.

into the tumor following the plan designed via preoperative CT. Then nitrogen or argon is delivered into the cryoprobe, where it expands into a gaseous state at the end of the cryoprobe and the temperature drops to around –180 °C. A thawing phase is followed, replacing the liquefied gas with helium or internally heating the probe. Freeze-thaw cycles are then repeated to obtain effective ablation. Thus effective preoperative planning is crucial for successful liver tumor cryoablation.

However, conventional empirically dependent planning is challenging since the optimal plan needs to consider complex clinical constraints, such as covering the entire tumor, ablating minimal healthy tissue, and avoiding surrounding organs. Under such rigorous clinical constraints, several works attempt to design automatic planning algorithms via finite-element method [1], set-cover [12], Pareto optimization [1, 13], heuristic method [11] and so on [8, 20]. However, these optimization-based algorithms almost down-sample the search space and ignore the interaction between probes, potentially leading to non-optimal results.

With the recent success of deep learning in medical image analysis [7, 9, 17], neural networks and reinforcement learning are further used to design planning algorithm [3, 5, 15]. Although these methods provide meaningful planning results, the precious annotations and lack of interpretability make them clinically impractical [11, 14]. **We instead formulate the probe insertion problem as the modeling of multiple regular ellipsoids, realized with parameterized differentiable 3D Gaussians, to collectively circumscribe the whole tumor. Motivated by the insertion logic of clinicians, our planning framework integrates the relationship between multiple probes.**

Specifically, we propose a 3D Differentiable-Gaussian-based Planning Strategy, named 3DGPS, targeting tumor cryoablation planning via preoperative CT. The method mainly consists of two stages: i) Fitting. The entire tumor is fitted with N ellipsoids controlled by our parameterized Gaussians with fitting loss and clinical constraints, where $1 \leq N \leq 4$ is based on clinical knowledge. ii) Circumscribing. Starting from fitting results, the N ellipsoids are then optimized by circumscribing loss and clinical constraints. The algorithm finally chooses the best plan under the consideration of several metrics. Particularly, we formulate and integrate the operating-specific and patient-specific knowledge in our loss function to make the optimized ellipsoid insertion feasible and in accord with the ablation goals. Therefore, our method possesses the following advantages:

– We formulate the probe insertion problem as the multiple regular circumscribed ellipsoid modeling, where the ellipsoids are parameterized with 3D

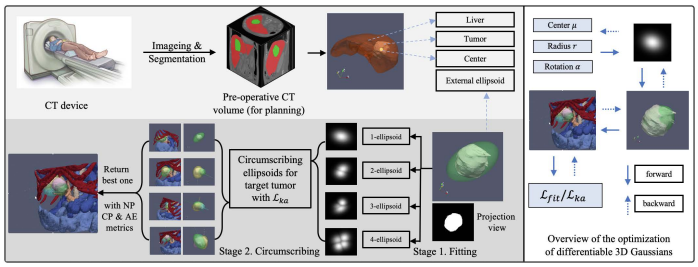

Fig. 2: The proposed planning framework mainly includes two stages, Fitting and Circumscribing. The fitting stage provides N fitted ellipsoids of the tumor, and the Circumscribing stage re-optimizes ellipsoids to circumscribe the tumor.

differentiable Gaussians. With further integration of the modified Khachiyan's algorithm, 3DGPS is capable of circumscribing the target tumor.
– 3DGPS builds the relationship between probes when more than one probe is necessary. Therefore, it's capable of providing the optimal number choice and the trajectory information, along with alternative suboptimal plans.
– Quantitative and qualitative experimental results on LiTS [2] and the in-house real-world datasets verify the effectiveness of 3DGPS. Besides, for the in-house data, We compare it with the results of cryoablation performed by real clinicians, and 3DGPS obtains high evaluation scores from clinicians.

2 Methodology

In this section, we concretely introduce the 3DGPS. As in Fig. 2, 3DGPS begins with Stage 1 which provides $1 \leq N \leq 4$ fitted ellipsoids of the whole tumor. Since 4 probes are the practical limit, we therefore provide 4 corresponding planning results. Then, in Stage 2, the ellipsoids are re-optimized to together circumscribe the tumor. We finally choose the best case based on several metrics. Next, we formulate the objective, followed by explaining the included stages.

2.1 Problem formulation

The cryoablation aims to cover the whole tumor while minimally ablating the surrounding healthy tissues. Particularly in previous works, ice balls are mathematically realized with regular ellipsoids ignoring the heat interaction. Based on the observations, we formulate the insertion planning as the modeling of multiple regular ellipsoids, which together circumscribe the whole tumor:

$$\begin{aligned} \min_{\{Q_i\}_{i=1}^{N}} \quad & \sum_{i=1}^{N} -\log\det Q_i \\ s.t. \quad & q_j^T Q_i q_j \leq 1, \exists \text{ i and } \forall q_j \text{in the target tumor}, \\ & Q_i \in R^{n\times n} \text{ is symmetric and positive definite}, \end{aligned} \tag{1}$$

where $\{Q_i\}_{i=1}^N$ are the parameterized decision matrix of the ellipsoids to be optimized, and N represents the probe number, i.e. the number of ice balls, which is decided in our planning under the consideration of several metrics.

2.2 3D differentiable-Gaussian-based planning algorithm

Directly solving the multiple-objective optimization problem is computationally expensive [13]. We instead employ 3D differentiable Gaussians to parameterize the ellipsoids and optimize the objective within two stages, as in Fig. 2.

3D differentiable-Gaussian-based ellipsoid. Firstly, the key point is how to parameterize the ellipsoids. Unlike implicitly modeling the ellipsoid with reinforcement learning [3] or neural networks [15], we propose explicitly modeling it with the parameterized 3D Gaussian distributions considering the planning interpretability. Especially, the ellipsoid decision matrices are mathematically decided by the centers $\{c_i\}_{i=1}^N$, radius $\{r_i\}_{i=1}^N$, and rotations $\{\alpha_i\}_{i=1}^N$. Then we map these parameters to the means $\{\mu_i\}_{i=1}^N$ and variance matrices $\{\sigma_i\}_{i=1}^N$, resulting the 3D differentiable Gaussians. In this way, once we feedback the updated parameters under the guidance of designed loss functions, these Gaussians would change, resulting in the expected ellipsoids of the planning.

Stage 1. Fitting. To efficiently optimize the involved parameters, we utilize the SGD under the PyTorch framework. Nevertheless, randomly initialized 3D Gaussian parameters may empirically lead to unstable and non-convergent results if we circumscribe the model directly. Therefore we design the fitting stage to provide initialized $1 \leq N \leq 4$ ellipsoids for further circumscribing. Targeting this, we first pre-circumscribe the whole tumor with a large ellipsoid, where the circumscribing problem reduces to the simplified form of objective (1), i.e., $N = 1$. For optimization, we employ the modified Khachiyan's algorithm [19] and re-implement it with PyTorch framework. Instead of iteratively computing the variable p^k in the original algorithm, we redesign the following loss function:

$$\mathcal{L}_{ka}(G_p^l) = \underbrace{\|G_p^l(g > \tau_G)\|_1}_{\text{inward loss}} + \underbrace{\lambda\|\mathbf{ReLU}(\tau_G - G_p^l \times T)\|_2}_{\text{outward loss}}, \tag{2}$$

where G_p^l is the predicted Gaussian, T is the tumor, g represents the probability value, $\mathbf{ReLU}$ is the operator from [4], τ_G is a controllable threshold, and λ is the balancing parameter, which is set to be a relatively large value. In this manner, when the ablation region does not cover the entire tumor, the outward loss dominates the optimization, enlarging the region. Otherwise, the outward loss tends to 0 and the inward loss dominates the optimizing, shrinking the region.

With the obtained probability density function (PDF) from pre-circumscribing, we then accomplish the fitting by employing the PDF-based method induced from the above G_p^l. To be specific, we first sample multiple centers $\{c_i\}_{i=1}^N$ from the PDF, followed by parameterizing corresponding Gaussian distributions centered at $\{c_i\}_{i=1}^N$. Then we fit these new distributions to cover the tumor under the clinical conditions with the following loss:

$$\mathcal{L}_{fit} = \|\mathbf{Max}_{i=1}^N(G_p^i) - T\|_2 + \beta\mathcal{L}_{sug}, \tag{3}$$

Table 1: Clinical limited conditions to be satisfied.

Clinical constraints	Notation
1. The **angle** between probe and normal vector at the entry point on the patient skin is less than τ_A.	A_{pre}
2. The probe & ice balls should avoid other **organs**.	O
3. The **ratio** among the three axes of the ellipsoid is constrained to be 5:3:3 depending on the property of the clinical probe.	ra

where $\mathbf{Max}(\cdot)$ represents the operation of taking the maximum value of $\{G_p^i\}_{i=1}^N$ and β is the balancing parameter. In this way, the first term enables these ellipsoids to fit with the tumor, and the second one is constrained by clinical conditions, which will be introduced later. Note that the target here is not finding the best-circumscribed ellipsoids but the ellipsoids that together match the whole tumor, i.e. achieving the best IoU. Intuitively, the fitting stage tries to model the interaction among ellipsoids, just like how to place each ellipsoid in the tumor to reach the best fit without considering the circumscribing rule.

Stage 2. Circumscribing. From these initialized ellipsoids, we next aim to further optimize them to satisfy the objectives (1) and accord with clinical conditions, providing the final ice balls. In particular, we utilize the following loss:

$$\mathcal{L}_{cs} = \mathcal{L}_{ka}(\mathbf{Max}_{i=1}^{N}(G_p^i)) + \gamma \mathcal{L}_{sug} \tag{4}$$

where γ is the balancing parameter. With the 4 different optimized results, under the empirically clinical constraints, we choose the best case according to several metrics (NP, CP, ATR), which will be introduced later. Therefore, we obtain the final plan from the physical information of the ellipsoid(s).

2.3 Clinical constraints formulation

The clinical scenario is very limited since the tumor location is close to various anatomies and the trajectory of probes should also avoid them, leading to the formulated clinical conditions in Table. 1. The violation between the optimized ellipsoid and such conditions would bring operating difficulties for clinicians. Therefore, we further formulate these as the following loss functions of constraints and integrate them in the optimization:

$$\begin{cases} \mathcal{L}_{angle} = \|\mathbf{ReLU}(A_{pre} - \tau_A)\|_2, \\ \mathcal{L}_{overlay} = \|\mathbf{ReLU}(\mathbf{Max}_{i=1}^{N}(G_p^i) \times O - \tau_G)\|_2, \\ \mathcal{L}_{probe} = \|\mathbf{Dismap}(O) \times \mathbf{ReLU}(\log(\tau_d) - \log(\mathbf{Dis}(o, \mathbf{L}(\sigma_i))))\|, \text{for } 1 \le i \le N \end{cases}$$

where, A_{pre}, O is in Table. 1, τ_A, τ_G and τ_d are corresponding thresholds, **Dismap** is the operation of obtaining distance map, o is internal points of organs, $\mathbf{L}$ is the operation of longest axis of $\sigma_i (1 \le i \le N)$, and **Dis** is the distance from a point to a line. The three radii of Gaussian are parameterized with the specific ratio 5:3:3. These together accomplish the constraints in Table. 1.

Table 2: Quantitative results on LiTS dataset and IH dataset. Note that N/A denotes there is no applicable results for the index.

LiTS	**Tumor** mm	**Plan**	**NP**	**AR** mm	**CP** %	**ATR↓** %	**IoU** %	**RE↑** (1-5)	**Time** min
P7	(41.0, 28.4, 24.0)	A	4	(35.5, 61.7, 33.3, 0)	100	76.40	N/A	2	6
		B	3	(46.8, 30.3, 34.5)	100	**58.03**	N/A	4	58
		C	4	(38.2, 33.3, 37.7, 36.4)	100	61.52	N/A	**5**	43
P9	(36.2, 27.8, 22.4)	A	3	(51.6, 0, 35.8)	100	69.44	N/A	4	5
		B	1	(55.0)	100	72.72	N/A	4	16
		C	4	(33.6, 31.4, 30.0, 33.4)	100	**58.83**	N/A	**5**	33
P17	(27.8, 21.6, 21.4)	A	4	(31.7, 31.7, 30.8, 32.6)	100	55.61	N/A	4	13
		B	1	(41.1)	100	**54.93**	N/A	**5**	70
		C	1	(41.1)	100	**54.93**	N/A	**5**	26
P19	(46.6, 25.4, 16.8)	A	4	(37.6, 0, 65.8, 0)	100	91.16	N/A	**4**	6
		B	2	(51.0, 53.0)	100	89.53	N/A	**4**	60
		C	3	(40.0, 39.0, 41.8)	100	**83.28**	N/A	**4**	35
P69	(26.2, 18.2, 15.2)	A	4	(27.2, 24.2, 23.7, 25.3)	100	57.02	N/A	1	4
		B	3	(22.3, 41.9, 41.0)	100	82.85	N/A	**4**	24
		C	4	(27.4, 25.6, 21.0, 23.8)	100	**54.07**	N/A	**4**	21
IH									
P1	(27.7, 24.5, 19.0)	A	4	(35.0, 33.4, 31.9, 34.0)	100	62.17	45.93	1	11
		B	3	(41.9, 28.2, 3.5)	100	63.09	46.34	3	41
		C	4	(32.6, 29.6, 29.8, 27.4)	100	**56.69**	49.96	**4**	37

3 Experimental results

Dataset. We first use the open LiTS [2] dataset to verify the performance of 3DGPS. Specifically, we select 5 tumors from 5 patients randomly, labeled as Pn where n represents the patient ID. Then we conduct experiments on one clinical case from our in-house dataset to compare with the practical ablation efficiency (conducted empirically by clinical doctors), which is rarely used in previous works. This retrospective study was conducted following ethical approval from the Institutional Review Board of Cancer Hospital, Chinese Academy of Medical Sciences.

Preprocessing. The **17** surrounding anatomies (spleen, right & left kidneys, gallbladder, stomach, pancreas, right & left lungs, esophagus, small bowel, duodenum, colon, vertebrates, aorta, vena cava, portal vein, and ribs), which affect the operating procedure, are segmented automatically by nnUNet [7] pre-trained on TotalSegmentator [21] and finally refined and confirmed by radiologist.

Evaluation. To verify the planning effectiveness, we qualitatively and quantitatively evaluate the results. For the metrics, we consider the Number of Probes (NP), Ablation Radius (AR), Coverage Percentage (CP), Ablated Tissue Ratio (ATR, ablated non-tumor tissue volume / tumor volume), Intersection over Union (IoU, only on IH dataset), Radiological Evaluation (RE), and running time.

Baselines. For a comprehensive comparison, we involve three plans, named Plan A, B, and C. Specifically, Plan A is the fine-tuned fitting results from the output

Table 3: Analysis of different numbers of probes in proposed Plan C.

LiTS	Tumor mm	Plan	#P	AR mm	CP %	ATR↓ %	IoU %	RE↑ (1-5)	Time min
P19	(46.6, 25.4, 16.8)	C	1	(67.6)	100	90.56	N/A	2	12
		C	2	(49.4, 41.2)	100	85.00	N/A	**5**	31
		C	3	(40.0, 39.0, 41.8)	100	**83.28**	N/A	4	35
		C	4	(38.8, 39.4, 39.6, 36.4)	100	85.88	N/A	4	36
IH									
P1	(27.7, 24.5, 19.0)	C	1	(48.8)	100	72.66	69.37	**5**	12
		C	2	(38.9, 39.2)	100	63.05	57.09	4	21
		C	3	(37.3, 34.0, 37.1)	100	64.95	51.97	4	30
		C	4	(32.6, 29.6, 29.8, 27.4)	100	**56.69**	49.96	4	37

of Stage 1, which enlarges the radii of each ellipsoid to make the output region cover the whole tumor. In Plan B, the whole tumor is divided into N parts based on the fitting results and we search the circumscribing ellipsoid for each part individually in Stage 2. In Plan C, we target to optimize N ellipsoids simultaneously to make the combined region circumscribe the whole tumor. Obviously, Plan B lack the interaction modeling between probes during the circumscribing stage.

Implementation details. All these automatic plans are implemented using PyTorch framework and trained on a NVIDIA 4090 GPU card with 100 iterations for fitting and 500 for circumscribing. We use Adam optimizer [10] with (β_1, β_2) = (0.9, 0.999). The learning rates of the optimizer are set to be $lr = 1.0$ for both fitting and circumscribing. The involved parameters $[\tau_G, \tau_A, \tau_d, \lambda, \beta, \gamma]$ is empirically set to $[0.4, 45, 5, 1e^6, 1e^8, 1e^8]$, respectively. Considering the elasticity of the skin and clinical usability, A_{pre} is implemented as the angle between the Y-axis and the projection of the probe direction to the YoZ plane, where the axes XYZ are depicted in Figure. 2.

3.1 Results analysis

Quantitative and qualitative results. We first quantitatively compare the three cryoablation plans and show the results in Table. 2. All three plans successfully cover the whole tumor but with different NP and ATR. Considering clinical requirements, such as minimizing ATR, less NP, and avoiding organs, an interventional radiologist provides the evaluation scores (RE) for each plan under the guidance of clinician evaluation procedures (Tables in supplementary material). As shown, Plan A is unstable and even violates organs on P69, resulting in the lowest RE score. While the circumscribing-based Plan B and C both robustly achieve better results. Especially with further interactivity modeling between ellipsoids, Plan C performs better in most cases. For the private IH dataset, a similar phenomenon is also observed and Plan C also achieves the best ATR and RE score. Further, we compare with practical results from the clinicians, i.e. the post-operative CT volume, and compute the IoU between our planning ablation

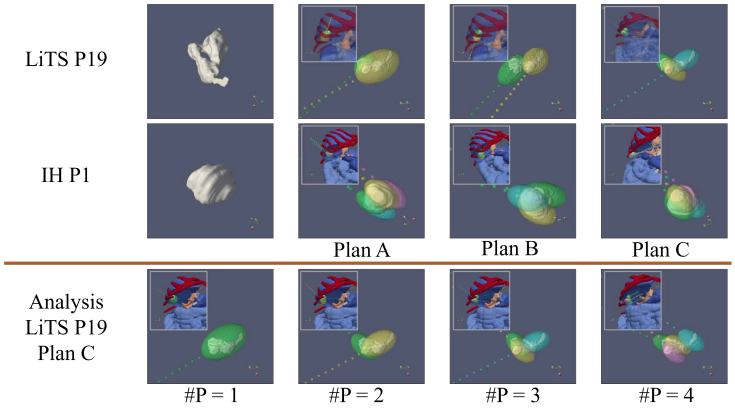

Fig. 3: The visualization of 3DGPS planning results on LiTS and IH datasets. Furthermore, we analyze Plan C on the P19 case of LiTS in detail.

zones and **their ablation zone** (**(95.06, 74.64)** for CP and ATR due to the clinical limit). Plan C seems closest to the clinical decision. Moreover, Plan C is better at covering the whole tumor even with such hard clinical constraints. Next, we visualize the planning results of three plans in Fig. 3, and Plan C shows better insertion conditions with lower challenge and smaller ablated volume.

Analysis of Plan C. Furthermore, we analyze Plan C in detail and show the quantitative results of the planning with different number of probes, denoted as #P, in Table. 3. Although Plan C achieves the best ATR when #P=4, the RE is lower than that case when #P=1. which is caused by the fewest probes, leading to better patient safety. Besides, Plan C with #P=1 achieved the highest IoU. With such analysis, we conclude that the planning evaluation is quite complex, and our planning is capable of providing alternative plans with different numbers of probes, which is rarely discussed previously.

4 Conclusion and Discussion

Targeting tumor cryoablation while minimally damaging surrounding healthy tissues, we formulate the problem as a multi-ellipsoids circumscribing problem. By introducing 3D differentiable Gaussians and fitting stage, we explicitly model ellipsoids and provide a meaningful planning procedure. Experiments on LiTS & IH datasets confirm the practical feasibility under various clinical constraints.

The proposed 3DGPS is not only an automatic planning algorithm considering both the probe interaction and clinical constraints, but also an open framework that can be applied to diverse clinical scenarios with minimal adaptions. For example: i) In cases where **the tumor size is too large**, it is impossible to cover the entire tumor within a limited number of probes. The planning objective will change such that most planning methods are no longer applicable. However,

in our framework, the fitting stage output can be used as the outcome of this objective, providing the best-fitted matchment. ii) Clinically, a plan with fewer probes causes less patient injury burden, inducing a strategy called **pull-back**, which means generating two ice balls with one inserted probe. Intuitively, it's feasible to introduce the strategy into our framework by just formulating the process as the integrated constraints. iii) Our framework can be directly generalized to kidney and other tumor ablation. Further, our method is modality-agnostic and can be applied to other modalities, e.g. MRI. Therefore, 3DGPS is an open framework that can be adjusted to various clinical scenarios. Further, the tumors in this study are almost less than 5 cm and relatively distant from the hilum, and the intrahepatic small vessels in these regions typically have diameters not exceeding 5 mm. Consequently, the prognosis for ablating intrahepatic small vessels in clinical practice appears to be manageable with minimal adverse events. To successfully apply our planning algorithm in practical surgeries, we will integrate navigation techniques in the whole surgery pipeline in the future.

Acknowledgments. We thank Dr. Hu Han and Dr. Hua Li for providing constructive suggestions on the organization and elaboration of the paper. We also thank Dr. S. Kevin Zhou for discussing this issue. This study was funded in part by the Innovation Team and Talents Cultivation Program of the National Administration of Traditional Chinese Medicine (No: ZYYCXTD-D-202202), in part by the National Natural Science Foundation of China (NSFC) under Grant No. 62271509, No. 62303438, and No. 62301532, in part by the Natural Science Foundation of Jiangsu Province of China under Grant No. BK20230282, and in part by the Joint Funds for the Innovation of Science and Technology of Fujian Province of China under Grant No. 2019KJCX068.

Disclosure of Interests. The authors have no competing interests to declare that are relevant to the content of this article.

References

1. Altrogge, I., Kröger, T., Preusser, T., Büskens, C., Pereira, P.L., Schmidt, D., Weihusen, A., Peitgen, H.O.: Towards optimization of probe placement for radio-frequency ablation. In: Medical Image Computing and Computer-Assisted Intervention–MICCAI 2006: 9th International Conference, Copenhagen, Denmark, October 1-6, 2006. Proceedings, Part I 9. pp. 486–493. Springer (2006)
2. Bilic, P., Christ, P., Li, H.B., Vorontsov, E., Ben-Cohen, A., Kaissis, G., Szeskin, A., Jacobs, C., Mamani, G.E.H., Chartrand, G., et al.: The liver tumor segmentation benchmark (lits). Medical Image Analysis **84**, 102680 (2023)
3. Chaitanya, K., Audigier, C., Balascuta, L.E., Mansi, T.: Automatic planning of liver tumor thermal ablation using deep reinforcement learning. In: International Conference on Medical Imaging with Deep Learning. pp. 219–230. PMLR (2022)
4. Glorot, X., Bordes, A., Bengio, Y.: Deep sparse rectifier neural networks. In: Proceedings of the fourteenth international conference on artificial intelligence and statistics. pp. 315–323. JMLR Workshop and Conference Proceedings (2011)
5. He, K., Liu, X., Shahzad, R., Reimer, R., Thiele, F., Niehoff, J., Wybranski, C., Bunck, A.C., Zhang, H., Perkuhn, M.: Advanced deep learning approach to automatically segment malignant tumors and ablation zone in the liver with contrast-enhanced ct. Frontiers in Oncology **11**, 669437 (2021)

6. Hu, K.Q.: Advances in clinical application of cryoablation therapy for hepatocellular carcinoma and metastatic liver tumor. Journal of clinical gastroenterology **48**(10), 830–836 (2014)
7. Isensee, F., Jaeger, P.F., Kohl, S.A., Petersen, J., Maier-Hein, K.H.: nnu-net: a self-configuring method for deep learning-based biomedical image segmentation. Nature methods **18**(2), 203–211 (2021)
8. Jaberzadeh, A., Essert, C.: Pre-operative planning of multiple probes in three dimensions for liver cryosurgery: comparison of different optimization methods. Mathematical Methods in the Applied Sciences **39**(16), 4764–4772 (2016)
9. Jin, K.H., McCann, M.T., Froustey, E., Unser, M.: Deep convolutional neural network for inverse problems in imaging. IEEE transactions on image processing **26**(9), 4509–4522 (2017)
10. Kingma, D.P., Ba, J.: Adam: A method for stochastic optimization. arXiv preprint arXiv:1412.6980 (2014)
11. Li, R., An, C., Wang, S., Wang, G., Zhao, L., Yu, Y., Wang, L.: A heuristic method for rapid and automatic radiofrequency ablation planning of liver tumors. International Journal of Computer Assisted Radiology and Surgery pp. 1–9 (2023)
12. Liang, L., Cool, D., Kakani, N., Wang, G., Ding, H., Fenster, A.: Automatic radiofrequency ablation planning for liver tumors with multiple constraints based on set covering. IEEE transactions on medical imaging **39**(5), 1459–1471 (2019)
13. Liang, L., Cool, D., Kakani, N., Wang, G., Ding, H., Fenster, A.: Multiple objective planning for thermal ablation of liver tumors. International Journal of Computer Assisted Radiology and Surgery **15**, 1775–1786 (2020)
14. Loftus, T.J., Tighe, P.J., Filiberto, A.C., Efron, P.A., Brakenridge, S.C., Mohr, A.M., Rashidi, P., Upchurch, G.R., Bihorac, A.: Artificial intelligence and surgical decision-making. JAMA surgery **155**(2), 148–158 (2020)
15. Meister, F., Audigier, C., Passerini, T., Lluch, È., Mihalef, V., Maier, A., Mansi, T.: Fast automatic liver tumor radiofrequency ablation planning via learned physics model. In: International Conference on Medical Image Computing and -Assisted Intervention. pp. 167–176. Springer (2022)
16. Nault, J.C., Sutter, O., Nahon, P., Ganne-Carrié, N., Séror, O.: Percutaneous treatment of hepatocellular carcinoma: state of the art and innovations. Journal of hepatology **68**(4), 783–797 (2018)
17. Ronneberger, O., Fischer, P., Brox, T.: U-net: Convolutional networks for biomedical image segmentation. In: Medical Image Computing and Computer-Assisted Intervention–MICCAI 2015: 18th International Conference, Munich, Germany, October 5-9, 2015, Proceedings, Part III 18. pp. 234–241. Springer (2015)
18. Shiina, S., Sato, K., Tateishi, R., Shimizu, M., Ohama, H., Hatanaka, T., Takawa, M., Nagamatsu, H., Imai, Y., et al.: Percutaneous ablation for hepatocellular carcinoma: comparison of various ablation techniques and surgery. Canadian Journal of Gastroenterology and Hepatology **2018** (2018)
19. Todd, M.J., Yıldırım, E.A.: On khachiyan's algorithm for the computation of minimum-volume enclosing ellipsoids. Discrete Applied Mathematics **155**(13), 1731–1744 (2007)
20. Torricelli, M., Ferraguti, F., Secchi, C.: An algorithm for planning the number and the pose of the iceballs in cryoablation. In: 2013 35th Annual International Conference of the IEEE Engineering in Medicine and Biology Society (EMBC). pp. 4949–4952. IEEE (2013)
21. Wasserthal, J., Breit, H.C., Meyer, M.T., Pradella, M., Hinck, D., Sauter, A.W., Heye, T., Boll, D.T., Cyriac, J., Yang, S., Bach, M., Segeroth, M.: Totalsegmen-

tator: Robust segmentation of 104 anatomic structures in ct images. Radiology: Artificial Intelligence **5**(5), e230024 (2023)